Aeroacoustics Conferences
26-29 May 2026, Brussels, Belgium
32nd AIAA/CEAS Aeroacoustics Conference (2026)

10.2514/6.2026-3443

Falcon 9 Noise Characterization from Two Measurement Campaigns

Makayle S. Kellison[1], Kent L. Gee[2], Grant W. Hart[3]
Department of Physics and Astronomy, Brigham Young University, Provo, Utah, 84602, USA

This paper presents an aeroacoustic analysis of SpaceX's Falcon 9 using data from two launches at Vandenberg Space Force Base. Acoustic measurements from 28 stations, ranging from 0.2 – 38.6 km, captured four key events: ignition overpressure, maximum launch noise, flyback sonic boom, and maximum landing noise. Sound exposure spectra show that the launch noise has a peak frequency of 30 Hz, an order of magnitude greater than the flyback boom peak frequency. Maximum 1-s overall sound pressure levels approach 150 dB at the closest stations and collapse well between launches across the full measurement range. Scientific Acoustic Tool for Understanding Rocket Noise (SATURN) predictions for launch noise in the time and frequency domains agree well with measured data, validating the recently developed model for Falcon 9. Using stations within 1 km, Falcon 9 was found to have a wide peak directivity region, spanning angles from 60 to 70°. The measured directivity angles are within the range of convective Mach number predictions and provide evidence that supersonic instability waves contribute to the main radiation lobe for rockets. Overall sound power levels were also calculated, producing an average sound power level of 195.4 $\pm$ 0.7 dB (1σ) and an acoustic efficiency of 0.30%. Sound power spectra peak at a Strouhal number of 0.010, lower than typical rocket assumptions and far below values for other supersonic jets. Overall sound pressure levels scaled to 100 nozzle diameters were similar to lower Mach number jets, suggesting that this metric may plateau at rocket-like conditions. These analyses extend understanding of the aeroacoustic source characteristics of rockets and better connect them to other supersonic, heated jets.

I. Nomenclature

c_a	=	ambient sound speed, m/s
c_e	=	plume exit sound speed, m/s
c_j	=	plume fully expanded sound speed, m/s
d	=	distance between the launch or landing pad and the stationary microphone, m
D_e	=	nozzle exit diameter, m
D_{eff}	=	effective exit diameter, m
D_j	=	fully expanded nozzle diameter, m
D_t	=	throat diameter, m
δ	=	ground reflection coefficient
F	=	thrust, N
f	=	frequency, Hz
γ_e	=	ratio of specific heats at exit
κ	=	convective velocity coefficient, U_c/U_j
L_{max}	=	maximum overall sound pressure level, dB re 20 μPa
L_p	=	frequency-dependent sound pressure level, dB re 20 μPa
$L_{p,\text{OA}}$	=	overall sound pressure level, dB re 20 μPa

[1] Graduate Student, Department of Physics and Astronomy, and AIAA Student Member.
[2] Professor, Department of Physics and Astronomy, and AIAA Associate Fellow.
[3] Associate Professor, Department of Physics and Astronomy.

L_w = frequency-dependent sound power level, dB re 1 pW
$L_{w,\mathrm{OA}}$ = overall sound power level, dB re 1 pW
M = convective Mach number (generic)
M_{ac} = jet acoustic Mach number, U_j/c_a
M_c = convective Mach number for supersonic instability waves
$M_c{}'$ = convective Mach number for Kelvin-Helmholtz instability waves
$M_c{}''$ = convective Mach number for subsonic instability waves
M_e = exit Mach number
M_j = fully expanded Mach number
M_κ = empirical convective Mach number
M_O = Oertel convective Mach number
n = number of engines
η = acoustic efficiency
P_e = exit pressure, Pa
P_j = fully expanded pressure, Pa
φ = azimuthal angle between the launch or landing pad and the stationary microphone, °
$Q(\theta, \mathrm{Sr})$ = frequency-dependent directivity index, dB
$Q_{\mathrm{max,OA}}$ = overall directivity index in the maximum radiation direction, dB
r = distance between the nozzle exit plane and the stationary microphone, m
Sr = Strouhal number, fD_e/U_e
σ = standard deviation
T_e = exit temperature, K
T_j = fully expanded temperature, K
θ = elevation angle between the jet axis and the stationary microphone, °
θ_M = maximum directivity angle derived from convective Mach number, °
U_c = convective velocity, m/s
U_e = nozzle exit velocity, m/s
U_j = fully expanded plume velocity, m/s
W = sound power, W
W_m = mechanical power, W
W_{ref} = reference sound power, 1 pW

II. Introduction

In the realm of supersonic jets, rockets represent the hottest and fastest of these propulsion systems and, as a result, generate the most noise. Early studies into launch vehicle noise, e.g. [1] [2] [3] [4] [5], culminated in NASA SP-8072 [6], a document that remains one of the most complete reviews of plume-induced acoustics today. In 2022, Lubert *et al*. [7] discussed needed updates to SP-8072 with new data from modern launch vehicles, but there remains a significant gap in understanding the aeroacoustic properties of rockets and how these vehicles fit into supersonic jet noise theory [7]. It is essential to understand the physics behind rocket noise generation as both launch cadence and vehicle thrust rapidly increase. The acoustics generated by a single rocket launch can have significant effects on structures [8] [9], endangered species [10] [11], and people living in surrounding communities [12], providing further motivation for the development of accurate source models.

Challenges associated with measuring a moving vehicle complicate the study of rocket source-level properties. McInerny *et al*. [13] [14] [15] [16] [17] identified four rocket noise characteristics that can be studied using far-field data and allow for rocket and supersonic jet acoustics to be studied within a common framework. These are directivity, overall sound power level ($L_{w,\mathrm{OA}}$), overall sound pressure level ($L_{p,\mathrm{OA}}$), and spectral peak frequency. In recent years, several studies have applied these techniques to modern launch vehicles, including Space Launch System (SLS) [18], Atlas V [20], and Delta IV Heavy [21].

This paper aims to further understanding of source level properties by studying the most frequently launched rocket: Falcon 9. As of April 2026, Falcon 9 versions have flown ~650 missions, including crewed missions to the International Space Station and deployment of commercial and government satellites. With its high launch cadence, Falcon 9 is the ideal candidate for additional noise study. Using acoustic data collected during two missions launched

from Vandenberg Space Force Base, measured Falcon 9 data are tied to rocket plume parameters through aeroacoustic analyses.

These results build upon the work of Mathews *et al*. [21], who characterized Falcon 9 far-field noise using measurements 6 – 12 km from the launchpad for three launches. Their paper presented both measurement results and a source analysis of Falcon 9, including the four aeroacoustic characteristics identified by McInerny. Here, these results are updated using a more extensive measurement campaign and data collected as close as 0.2 km from the launchpad. The near-pad locations and quantity of measurements provide a more detailed and accurate characterization of Falcon 9's noise generation and propagation.

The paper first describes the two large-scale measurement campaigns and presents results collected at the 28 measurement sites located 0.2 to 38.6 km from the launchpad. Four significant acoustic events are identified: ignition overpressure, maximum launch noise, flyback sonic boom, and maximum landing noise. Maximum launch noise and flyback sonic boom levels are compared as a function of distance to determine variation between launches. The measured launch noise data are then compared to predictions made using the Scientific Acoustic Tool for Understanding Rocket Noise (SATURN) [22]. Six of the 28 locations were less than 750 m from the launchpad, and these locations are used to extrapolate back to the source to connect Falcon 9's noise radiation to key plume parameters, as described by McInerny. First, overall and frequency-dependent directivity results are shown. Falcon 9's $L_{w,\mathrm{OA}}$ and acoustic efficiency, η, are updated based on new methodology and near-pad data. This technique is applied to every frequency band to find Falcon 9's Strouhal number-normalized sound power spectrum, which is compared to other launch vehicles and supersonic jets. Finally, $L_{p,\mathrm{OA}}$ scaled to 100 nozzle diameters (D_e) is given as a function of convective Mach number. Necessitated by Falcon 9's high launch cadence from three spaceports, this aeroacoustic analysis updates the results of Mathews *et al*. [21] with a more accurate acoustic source model and represents an additional effort to connect rocket noise with supersonic jet aeroacoustics.

III. Falcon 9 Launch Vehicle

Falcon 9 Block 5 is a medium-lift, two-stage rocket developed by Space Exploration Technologies Corporation (SpaceX). The first (booster) stage is powered by nine Merlin 1D liquid engines, which use cryogenic rocket-grade kerosene (RP-1) and liquid oxygen as propellant. Falcon 9 is shown lifting off with all nine engines ignited in Figure 1a. Each Merlin 1D engine produces 845 kN of thrust, for a combined liftoff thrust of 7.6 MN. Additional engine parameters for the Merlin 1D engine are shown in Table 1. Parameters were selected from publicly available information and derived from the Chemical Equilibrium with Applications (CEA) online program developed by NASA Glenn Research Center [23]. For detailed information regarding CEA model inputs, see the Appendix.

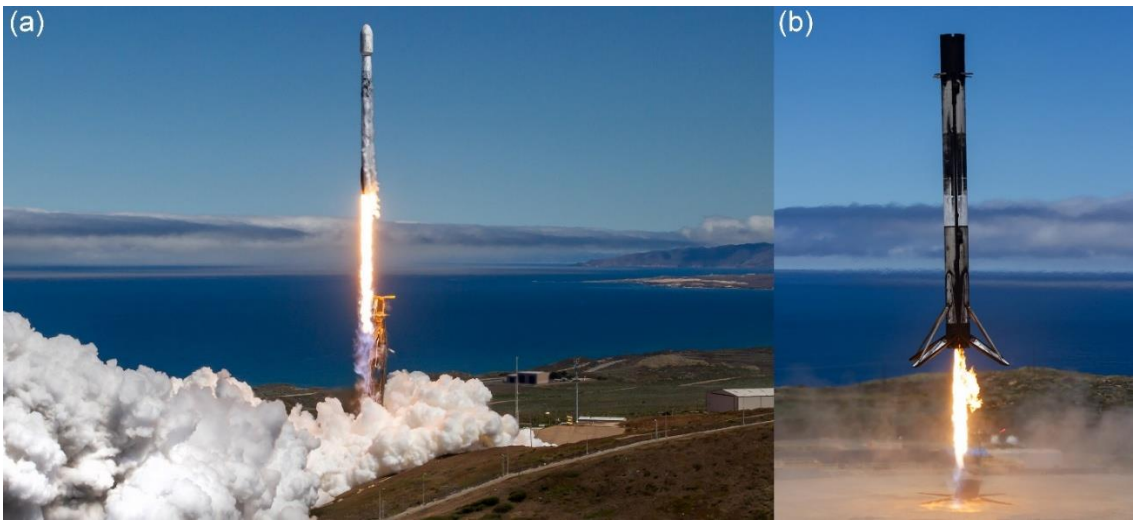

Figure 1. Falcon 9 during ascent at T+8 s, launching the TRACERS mission from SLC-4 at Vandenberg Space Force Base. Falcon 9 first-stage booster landing at LZ-4 at T+466 s (Photo Credit: SpaceX).

The Falcon 9 booster is designed for rapid reuse and has the capability to land vertically ~8 minutes after liftoff. Falcon 9 booster landings often occur downrange in the ocean on autonomous spaceport drone ships, but some missions include a return-to-launch-site (RTLS) landing. During first-stage flyback, a single Merlin engine reignites

~20 s before landing to slow the booster, allowing the four legs to deploy for a controlled vertical landing (see Figure 1b). As of April 2026, individual Falcon 9 boosters have flown as many as 34 missions. Both launch and landing events produce unique acoustic signatures that warrant detailed study.

Table 1. Engine parameters for Merlin 1D.

T_e	Exit temperature	1402 K
T_j	Fully expanded temperature	1532 K
P_e	Exit pressure	65,406 Pa
P_j	Fully expanded pressure	101,300 Pa
c_e	Exit sound speed	804 m/s
c_j	Fully expanded sound speed	838 m/s
U_e	Exit velocity	2984 m/s
U_j	Fully expanded velocity	2904 m/s
M_e	Exit Mach number	3.713
M_j	Fully expanded Mach number	3.465
γ_e	Ratio of specific heats at exit	1.257
D_e	Exit diameter	0.92 m
D_j	Fully expanded diameter	0.79 m
D_{eff}	Effective exit diameter	2.76 m
D_t	Throat diameter	0.23 m
F	Thrust	845 kN

IV. Measurement Description

Data used in this manuscript were collected during two Falcon 9 missions launched at Vandenberg Space Force Base (VSFB) in Santa Barbara County, California. The Tandem Reconnection and Cusp Electrodynamics Reconnaissance Satellites (TRACERS) mission was launched at 11:13 am PDT on July 23, 2025, and the National Advanced Optical System (NAOS) mission was launched at 11:53 am PDT on August 26, 2025. Falcon 9 launched from Space Launch Complex 4 (SLC-4) at VSFB for TRACERS and NAOS. Both missions included RTLS landings, where the first-stage booster touched down at Landing Zone 4 (LZ-4) approximately 400 m west of SLC-4.

Figure 2. Six measurement stations at TRACERS and NAOS relative to SLC-4 and LZ-4. Falcon 9 and booster are shown on the launch and landing pads, respectively, not to scale.

Twenty-eight measurement stations were deployed for each launch, ranging from 0.2 to 38.6 km from SLC-4. Measurement stations were placed in similar locations for each mission to capture any launch-to-launch variability in the far field. The initial analysis and SATURN predictions presented in the paper use all measurement stations. However, the source-level aeroacoustic analysis focuses on a subset of six stations, located less than 1 km from both SLC-4 and LZ-4. These stations are shown in Figure 2 and their distances and azimuthal angles are given in Table 2.

All measurement stations were comprised of a compact data acquisition system housed in a briefcase-sized Pelican case and referred to as the Portable Unit for Measuring Acoustics (PUMA). Data were collected using National Instruments 9250 and 9234 cards sampling at either 51.2 (distances > 5 km) or 102.4 (distances < 5 km) kHz. Free-field and pressure condenser microphones of various sensitivities (0.2 – 8 mV/Pa) were used due to the wide range of measurement distances. Stations located less than 1 km from SLC-4 or LZ-4 used GRAS 6.35 mm (¼ in) 46 BG (3.15 Hz to 70 kHz), BD (5 Hz to 70 kHz), and BE (4 Hz to 80 kHz) microphones. GRAS 47 AC (0.09 Hz to 20 kHz) or PCB 378A07 (0.13 Hz to 20 kHz) 12.7 mm (½ in) infrasound microphones were used at the remaining distances. To compensate for the roll-off in low-frequency response of the 6.35 mm microphones, a digital filtering technique (pole-shift filtering) was applied to all waveforms [24] [25]. This method has been used on various other rocket noise and sonic boom measurements to flatten the low-frequency response of the hardware. Microphones were set up inverted above a plastic ground plate and housed in a weatherproof foam windscreen [26]. PUMA systems with the same microphone configuration have been used in the measurement of several rockets, including SLS [27] and Starship Super Heavy [28]. Consistency in measurement approaches enables comparison of different vehicles and launches.

Table 2. Distances and azimuthal angles for a subset of measurement stations shown in Figure 2.

Station	d re SLC-4, m	φ re SLC-4, °	d re LZ-4, m	φ re LZ-4, °
10	750	357	750	30
11	455	40	751	71
12	240	107	667	105
13	285	157	641	125
14	703	291	282	300
15	652	325	430	5

V. Waveform and Spectral Characteristics

Falcon 9 launches with RTLS booster landings include multiple events of acoustical significance. Much of this manuscript will focus on the maximum launch noise, but all events are discussed in this section to demonstrate the unique acoustic behavior captured in the two missions. A pressure waveform is shown in Figure 3a from the TRACERS launch measured at Station 10, equidistant from SLC-4 and LZ-4 (750 m). The timing of four notable events is indicated by colored arrows, and their corresponding waveforms are shown in Figure 3b – e. Ignition overpressure (IOP) is displayed in Figure 3b and refers to the low-frequency pressure wave generated during Merlin engine ignition at T-3 s. The IOP's peak amplitude is ~20 Pa (120 dB), making it the event with the lowest acoustic levels. However, 20 Pa is equivalent to Falcon 9's peak levels measured at 10 km, where observers often view the launch. The IOP has been the subject of previous studies on launch vehicle noise and vibration [29] [30] and is often a highly directional event [7] [20], influenced by launch pad design (particularly the orientation of the flame trench). Station 10 is located ~357° relative to SLC-4 (north), whereas the flame trench opens south of the pad. As a result of the directional propagation, IOP levels recorded to the south at an equivalent distance are ~126 dB, nearly double that of the levels observed at Station 10. Additional IOP analyses are not discussed in this manuscript, but understanding the near- and far-field behavior of this event is important in future work and predictive models, particularly those focused on launchpad structural impacts.

Figure 3c highlights the waveform characteristics surrounding the maximum of the 1-s averaged $L_{p,\mathrm{OA}}$, where the peak pressure is ~540 Pa (149 dB peak sound pressure level). Distinct shocks dominate this waveform segment, demonstrating the nonlinear nature of the launch noise, which is perceived as crackle [31] [32]. These shocks are notably higher frequency than those produced by super heavy-lift vehicles, like SLS [27] or Starship Super Heavy [28]. This increase in peak frequency arises primarily due to the smaller effective exit diameter of the medium-lift Falcon 9. The effective exit diameter is defined as $D_{\mathrm{eff}} = D_e\sqrt{n}$, where n is the number of engines and D_e is the exit diameter of a single engine. The maximum landing noise, shown in Figure 3e, reaches amplitudes up to 156 Pa (138 dB peak level), 11 dB less than the maximum launch noise. This reduction in level can be attributed to only a single engine igniting during the landing burn. Nonetheless, landing noise has been shown to be of equal amplitude to launch noise for other rockets [28].

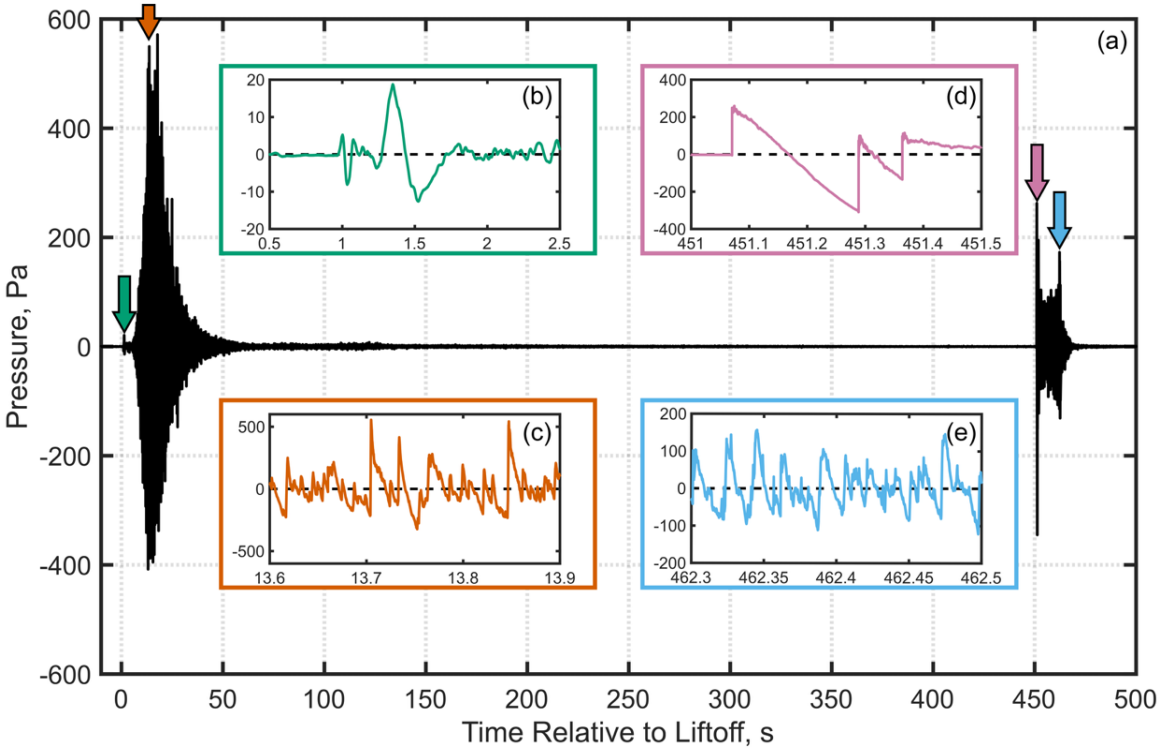

Figure 3. (a) Waveform at Station 10 (0.75 km from SLC-4 and LZ-4) for the Falcon 9 TRACERS launch, along with waveform segments during (b) ignition overpressure, (c) maximum launch noise, (d) flyback sonic boom, and (e) maximum landing noise. Subplots (b) – (e) are in units of pascals.

The flyback sonic boom, generated as the booster returns to earth at supersonic speeds, is shown in Figure 3d. Falcon 9 produces a sonic boom with three shocks during reentry due to the booster's geometry [33] [34]. This triple sonic boom reached a peak overpressure of ~250 Pa (5 psf and 142 dB peak level), significantly less than the maximum launch noise. This is likely due to the proximity of this measurement location to the launch and landing pads. Previous work [35] [36] has shown that the launch noise dominates as the most significant acoustic event at distances less than 1 – 2 km, whereas the sonic boom produces the greatest pressures at distances beyond this range.

Spectra at Station 10 corresponding to the four periods of interest are plotted in Figure 4. The maximum launch and landing noise segments were extended to provide greater low-frequency spectral resolution, and the flyback sonic boom was zero-padded for similar reasons. The Z-weighted (unweighted) sound exposure level spectrum is plotted for all four events, allowing for quantitative comparison between the continuous-noise and transient launch events. The IOP has the lowest peak frequency of 2 – 3 Hz, with relatively little spectral energy beyond 100 Hz. The maximum launch noise is more broadband, with significant energy present in the entire displayed spectral bandwidth. The launch noise peaks around 20 – 30 Hz, and contains significant high-frequency energy, characteristic of strong shocks. The flyback boom has a unique spectral shape, but a peak frequency nearly an order of magnitude less than the launch noise. The dominant spectral peak occurs at ~3 Hz. Similar results are reported in other Falcon 9 flyback boom spectra at less than 1 km [35] [36]. Finally, the maximum landing noise peaks at 70 – 80 Hz, significantly higher than the 20 – 30 Hz peak observed during launch. This shift is consistent with the transition from a nine-engine plume (launch) to a single-engine plume (landing). Since frequency scales inversely with plume diameter, the reduced plume size during landing should correspond to a factor of three increase in peak frequency. The landing noise also contains a similar high-frequency spectral shape as the launch noise from 100 Hz to 2 kHz at a reduced level. Above 2 kHz, the landing noise spectrum rolls off more quickly than both the launch noise and flyback boom spectra. Both launch noise and flyback boom events maintain a 10 dB per decade high frequency roll off across the entire frequency bandwidth in Figure 4, characteristic of ideal weak-shock behavior [37]. Presumably, the lower sound levels associated with landing result in less nonlinearity and greater impact of atmospheric absorption.

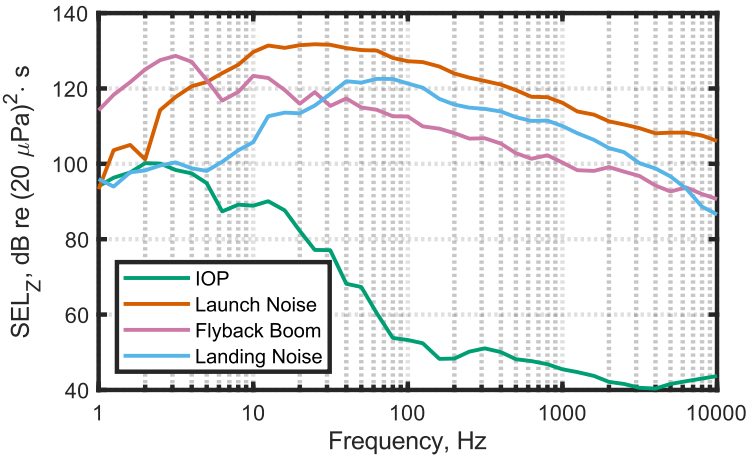

Figure 4. Sound exposure level spectra at Station 10 (0.75 km from SLC-4 and LZ-4) for the Falcon 9 TRACERS launch. The spectra correspond to the waveform segments of the four significant acoustic events noted in Figure 3, but the maximum launch and landing noise segments were extended to T+13-21 and T+460-464 s, respectively.

VI. Maximum Launch Noise and Flyback Sonic Boom Levels

The launch noise's unweighted maximum 1-s averaged $L_{p,\mathrm{OA}}$, referred to as $L_{\max}$ for the remainder of this paper, and the flyback sonic boom peak overpressure are of interest to understand the acoustic footprint of both launch and landing events. All measurement stations, from 0.2 to 36.8 km, are studied and compared between missions in this section. It is notable that the two farthest measurement locations were placed south of SLC-4, well beyond the borders of VSFB. These locations were along Falcon 9's southerly trajectory, and the vehicle has significantly pitched over when these stations receive their maximum launch noise.

Figure 5a shows the $L_{\max}$ at each location for the TRACERS (blue circles) and NAOS (yellow squares) missions. The predicted $L_{\max}$ is also plotted as a line using the most updated version of what is commonly referred to as the McInerny model [38]. This model is described by

$$L_{\max} = 10\log_{10}\left(\frac{\frac{1}{2}\eta F U_e n}{W_{\mathrm{ref}}}\right) - 10\log_{10}(4\pi r^2) + Q_{\max,\mathrm{OA}} + 20\log_{10}(\delta)\,. \tag{1}$$

The first term in Equation 1 is the predicted overall sound power level, where F is the thrust of one engine, U_e is the exit velocity, n is the number of engines, and W_{ref} = 1 pW. All other parameter values in Equation 1 were selected to match the most recent implementation of the McInerny model by Mathews and Gee [38]. The acoustic efficiency, η, represents the ratio of the rocket's sound power and mechanical power, and it is assumed to be 0.33%. The second term represents losses due to geometric spreading, where r is the distance from the vehicle nozzle exit plane to the measurement location. The third term accounts for the directionality of the source, where $Q_{\max,\mathrm{OA}}$ is the directivity index in the maximum radiation direction. Here, $Q_{\max,\mathrm{OA}}$ is assumed to be 5 dB. The final term accounts for pressure doubling experienced by ground-based observers, where $\delta = 1.9$.

There are three key results from Figure 5a. First, there is strong agreement between the two Falcon 9 measurements, even in the far field at 30+ km. This is often where the most variation is seen in acoustic levels due to time of day, weather, and seasonal differences in the atmosphere. TRACERS and NAOS were both launched between 11:00 am and 12:00 pm Pacific Time during the summer. For TRACERS, the local weather was 64.4° F with 68.0% relative humidity, and winds were 10 mph to the N. For NAOS, the local weather was 69.8° F with 68.6% relative humidity, and winds were 9 mph in the WNW direction. Despite these similarities, it is still surprising that $L_{\max}$ agree so strongly between missions. Prior rocket noise measurements [39] at these distances have shown strong disagreement (~30 dB) between repeated measurement locations at 30+ km. Second, the measured $L_{\max}$ match the

predictive model [38] well until ~4 – 5 km. Past this distance, the model tends to overpredict $L_{\max}$ because it does not account for absorption or other propagation losses that are likely reducing the high-frequency content of the launch noise. Third, because of the clustered symmetric arrangement of engines, there does not appear to be any clear azimuthal dependence on the vehicle's maximum launch noise.

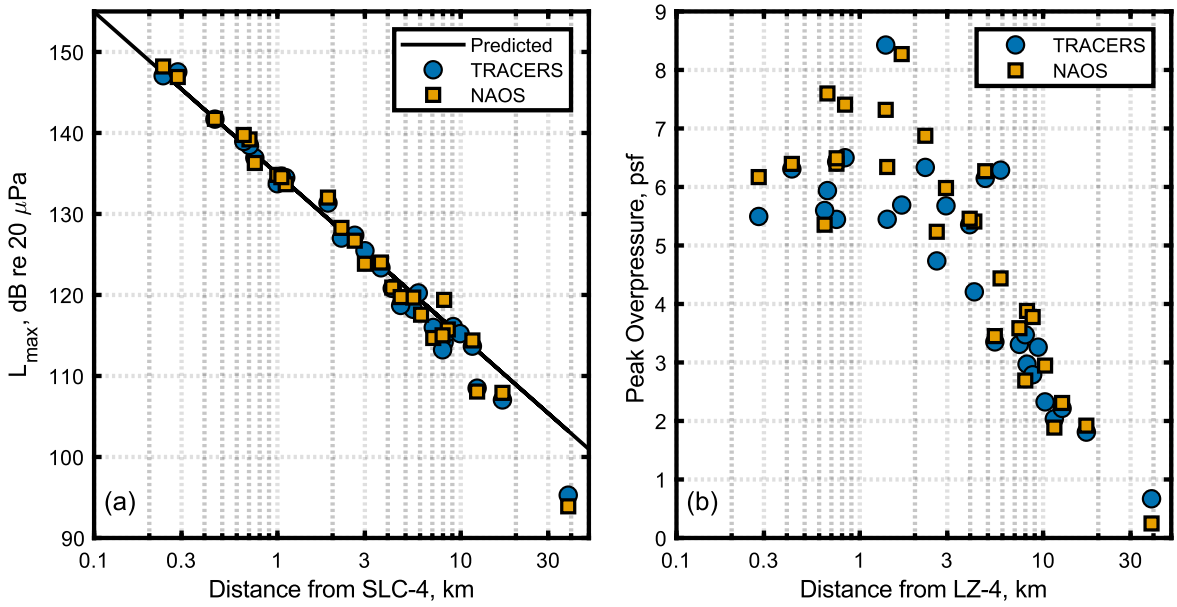

Figure 5. (a) Measured launch noise maximum overall sound pressure levels and (b) measured sonic boom peak overpressures for two Falcon 9 launches. Launch noise data in (a) are plotted with a prediction for Falcon 9 using Mathews and Gee [38].

Peak overpressures from the flyback sonic boom are reported in Figure 5b. Although this metric does not strictly correspond to human perception of rocket sonic booms [40], it is used here to provide comparisons to environmental and structural assessments. The sonic boom overpressure does not follow a clear exponential decay with distance, differing from the launch noise. The greatest overpressures of more than 8 pounds per square foot (psf) were recorded between 1 and 2 km from LZ-4, while microphones ~300 m from LZ-4 had peak overpressures around 6 psf. Anderson *et al*. published a similar figure for three other Falcon 9 booster landings at LZ-4 [41]. They report peak overpressures plateauing within 2 km from the landing pad, whereas the overpressures in Figure 5b increase and reach a visible peak between 1 – 2 km. This could be due to atmospheric turbulence, which causes focusing and defocusing of the sonic boom footprint, as well as differences in trajectory between launches.

VII. SATURN Predictions

The measurement results described in the previous sections provide a comparison point for current rocket noise modeling efforts. In this section, measured data are compared to a recently developed rocket noise model: the Scientific Tool for Understanding Rocket Noise (SATURN). SATURN incorporates models for sound power spectra and radiated directivity indices to predict noise radiation at any location. Studying source level aeroacoustic characteristics provides insights into the physical mechanisms behind rocket noise generation, which can eventually be implemented as SATURN improvements.

The ability to accurately model the generation and propagation of noise from a launch vehicle has been significantly improved by high-fidelity acoustic measurements of several modern launch vehicles. SATURN was developed using methods outlined in SP-8072 in conjunction with data collected from one Atlas V 401 launch [22]. The publicly available repository is simple compared to other rocket noise modeling tools (e.g., RUMBLE [42]) and provides a much more detailed, time and frequency-resolved prediction. SATURN requires a vehicle trajectory as well as engine parameters and uses these inputs to predict the acoustic levels (pressure and power) as a function of time or frequency at any specified location. The model has previously been validated against data collected for Firefly's Alpha and SpaceX's Starship Super Heavy [22].

SATURN is validated here for Falcon 9 using data from both TRACERS and NAOS. The engine parameters given in Table 1 are used as inputs for the model. Figure 6 compares measured data to SATURN predictions at three measurement locations: 1.1, 2.6, and 5.9 km. Both the running $L_{p,\mathrm{OA}}$ and the one-third-octave (OTO) band spectra, represented in autospectral density units, are plotted for each location. Overall levels are shown beginning at T+5 s because SATURN does not currently account for deflected plume and ground-level propagation effects [22].

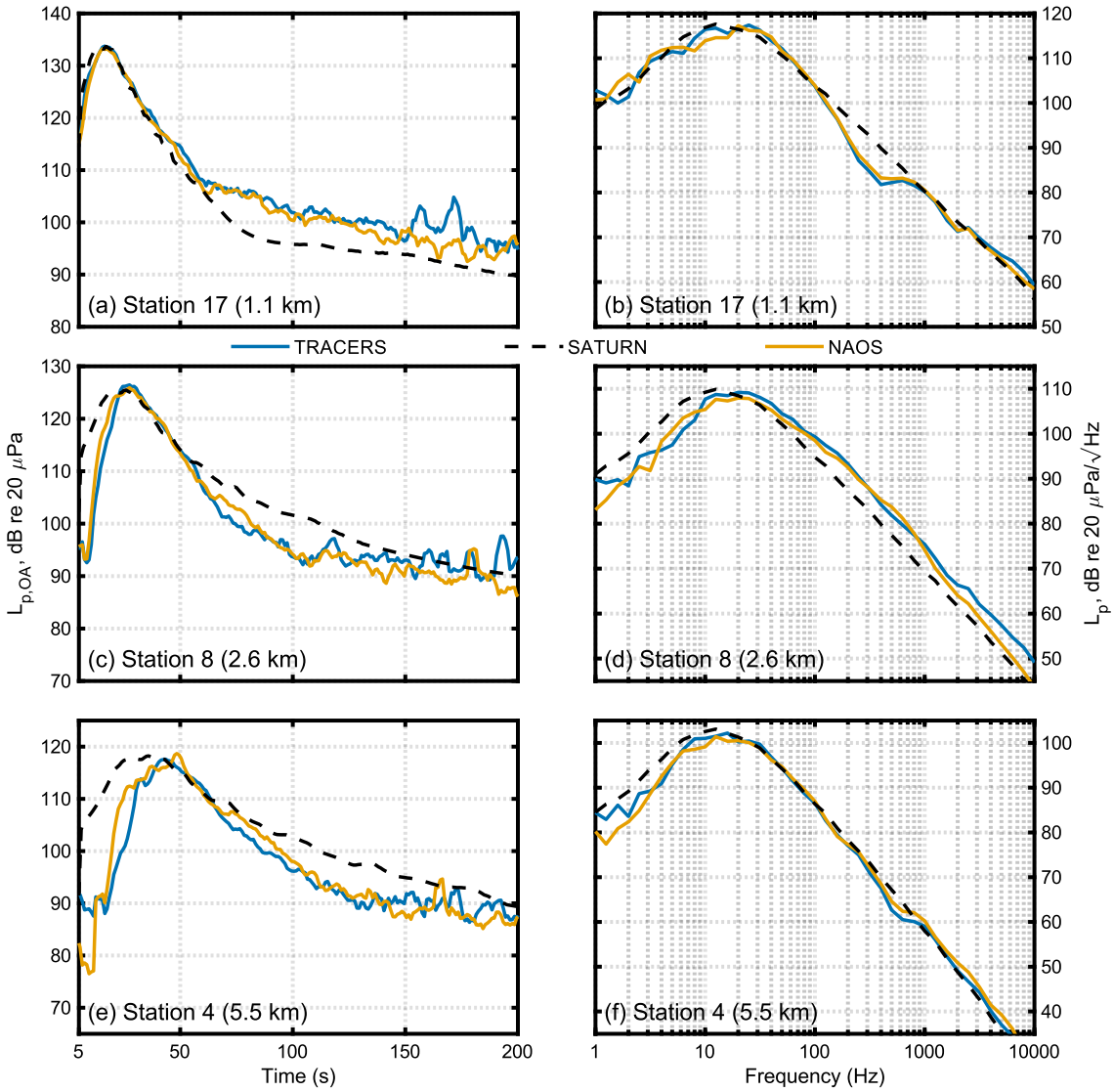

Figure 6. Measured Falcon 9 data from two launches and SATURN predictions for (a, c, e) running overall sound pressure levels and (b, d, f) maximum launch noise one-third-octave band spectra, represented in autospectral density units, at three representative distances.

Several observations are noted from Figure 6a, c, and e. At 1.1 and 2.6 km, the SATURN predictions and measured data agree very well with variation of less than 1 dB around the peak region. After ~100 s, SATURN slightly underpredicts the acoustic levels at 1.1 km and overpredicts the levels at 2.6 km, but there is significantly more fluctuation in the measured data in this range. This disagreement could be due to a variety of factors, including complex atmospheric turbulence and nonlinear propagation effects, neither of which are comprehensively accounted for in SATURN. At 5.9 km, SATURN overpredicts the $L_{p,\mathrm{OA}}$ during the first 40 s of launch. The maximum measured data arrive significantly later than predicted, reaching a sharp peak around 45 – 50 s, whereas SATURN shows a flatter peak beginning around 30 s. However, after 50 s, the model and measured data collapse remarkably well considering the distance from the launchpad. The initial discrepancy is likely due to terrain shielding line of sight from the

measurement location to the launchpad. Prior work [21] showed a reduction in $L_{p,\mathrm{OA}}$ and high-frequency content during first 50 s of launch for long-range measurements of Falcon 9 at VSFB. This work provides further motivation for ray-tracing methods to be applied to rocket noise and incorporated into SATURN.

SATURN's maximum OTO spectra in Figure 6b, d, and f are also compared to the measured spectra. All spectra are calculated over the 3 dB-down period relative to $L_{\max}$ and then converted to autospectral density units. At 1.1 km, the SATURN spectrum peaks around 12 Hz, whereas the measured data peak between 20 – 30 Hz. The overall spectra match well, despite a slight interference null in the measured data between 200 – 700 Hz. SATURN's spectral results at 2.6 and 5.9 km also agree well with the measured data. However, in both instances, SATURN overpredicts the low-frequency energy. SATURN should be validated with additional launch vehicles to determine the cause of this discrepancy.

VIII. Aeroacoustic Methods

The measurement results outlined in previous sections help quantify the spatial extent of rocket noise, showing that low-frequency liftoff noise remains audible out to at least ~38 km from the launchpad. Current rocket noise models, such as SATURN, provide fairly accurate spectrum- and time-resolved predictions of launch noise. However, SATURN remains an empirical model. To improve future modeling efforts, current measurements must be connected to supersonic jet noise and flow physics. A physics-based model would provide greater accuracy and be able to predict the noise from a rocket that does not yet exist.

With this broader goal in mind, physics-based predictions begin with an accurate source model of a full-scale rocket plume. Developing such a model is complicated by having a moving acoustic source and difficulties in making near-field measurements. However, several key aeroacoustic characteristics can be quantified from far-field data [14]. Six measurement stations used are located 240 – 750 m (87 – 271 D_{eff}) from the launchpad. While the geometric far-field (i.e., spherical spreading) onset is not well defined for rocket noise, these distances represent a reasonable effort to place microphones sufficiently far from the source to represent far-field behavior on average, yet close enough to minimize propagation effects that can influence source-related analyses. Here, the similarity of results from four key analyses across the stations suggests validity of a far-field assumption. Use of six stations inside 1 km provides an optimal dataset for source characterization and revises results provided by Mathews *et al*. [21] that used a limited dataset obtained at much greater distances. Measurement locations remained the same between the two Falcon 9 launches, TRACERS and NAOS, providing additional confidence in the results. First, acoustic and trajectory data are combined to determine the angle at which the maximum noise is emitted, known as the maximum directivity angle. The measured directivity is tied to convective Mach number theory, providing insight into the types of instability waves propagating into the acoustic field. The directivity function can be integrated to calculate Falcon 9's frequency-dependent sound power spectrum, L_w, or overall sound power level, $L_{w,\mathrm{OA}}$, and corresponding η. Although $L_{w,\mathrm{OA}}$ is the most accurate source metric, many studies in supersonic jet noise have instead compared different-sized jets using L_{max} at 100 D_{eff}. This metric is calculated for Falcon 9, allowing for additional comparison to supersonic jets of various sizes. All of these aeroacoustic analyses update initial results provided by Mathews *et al.* [21] for Falcon 9 and provide additional insight into how rockets fit into current supersonic jet noise theory.

IX. Directivity

Directivity is a fundamental aeroacoustic characteristic because it connects the radiated acoustic field to physical phenomena in the jet. Rocket noise originates from turbulent eddies within the plume. When these spatially coherent structures move fast enough, they become supersonic with respect to the medium (air) and radiate efficiently as Mach waves [43]. The convective Mach number relates the convection velocity U_c of these turbulent structures to the Mach wave radiation angle. The peak radiation direction of the jet occurs at the Mach wave angle,

$$\theta_M = \cos^{-1}\left(\frac{1}{M}\right), \tag{2}$$

where θ_M is measured relative to the plume centerline, and M is a general convective Mach number.

Different definitions of M have been proposed, ranging from physics-based to empirically derived equations. Early physics-based definitions were introduced through experiments by Ortel [44] [45] and connected to theory by Tam and Hu [46], leading to a velocity-based classification of instability waves within the jet plume. This framework

identifies three primary wave types: Kelvin-Helmholtz, supersonic, and subsonic instability waves. Kelvin-Helmholtz instability waves convect at the highest speeds and radiate at the farthest aft angles relative to the plume centerline. Supersonic instability waves convect slower and radiate at comparatively shallower angles. Although regarded as an internal, non-radiating class of waves, it is possible that even subsonic instability waves result in Mach wave radiation for a rocket. If they do radiate, subsonic instability waves travel the slowest and radiate at the shallowest angles

Due to their high convection speeds, Kelvin-Helmholtz instability waves are the first to couple with the surrounding fluid as jet velocity and temperature increase. This class of wave dominates the Mach wave radiation for a large range of supersonic jets, from laboratory scale up to full-scale military aircraft [47]. At afterburning conditions, full-scale military aircraft have high enough temperatures and velocities where supersonic instability waves also start to radiate. The fully expanded velocity, U_j, and, therefore, acoustic Mach number, $M_{ac} = U_j/c_a$, of rockets is significantly greater than even a military aircraft at afterburner [7]. Therefore, the main radiation lobe of a rocket plume could be comprised of both Kelvin-Helmholtz and supersonic instability waves. Each class of instability wave can be represented with a convective Mach number, where $M_c{}'$ is associated with Kelvin-Helmholtz instability waves, M_c corresponds to supersonic instability waves, and $M_c{}''$ represents subsonic instability waves.

This initial work inspired additional studies into convective Mach number. Greska *et al.* [48] [49] developed the Oertel convective Mach number, M_O, by taking the arithmetic mean of the Kelvin-Helmholtz and supersonic instability Mach numbers. Beyond radiation angle, M_O is used to identify patterns in distance corrected $L_{\max}$ for a wide range jets, from subsonic to rockets. This is discussed further in Section XI.

The final convective Mach number discussed in this paper is M_κ. For decades, the supersonic jet noise community has defined an empirical convective Mach number based on the convection velocity U_c being some fraction of the fully expanded velocity U_j. This ratio is defined as κ and the corresponding convective Mach number is $M_\kappa = \kappa U_j/c_a$. Values for κ depend on jet velocity and temperature, with laboratory scale jets having κ values of 0.6 – 0.85 and rockets found to have values closer to 0.3. Recently, Gee *et al.* [47] compiled data from a variety of supersonic jets, from laboratory-scale cold jets to full-scale rockets and determined that κ is approximately equal to $1/\sqrt{M_{\mathrm{ac}}}$ and $M_\kappa \approx \sqrt{M_{\mathrm{ac}}}$. Because M_κ can be tied to $M_c{}'$ mathematically, their investigation provides a more robust, physics-based definition of M_κ.

The equations for the five convective Mach numbers, $M_c{}'$, M_c, $M_c{}''$, M_O, and M_κ, are given in Table 3, along with their predicted θ_M for Falcon 9 using the jet parameters from Table 1. The predictions are compared to measured data from TRACERS and NAOS, discussed in the remainder of this section.

Table 3. Five convective Mach numbers expressed in terms of the acoustic Mach number, $M_{\mathrm{ac}} = U_j/c_a$, and their corresponding values for Falcon 9.

	Definition	M	θ_M
$M_c{}'$	$\dfrac{M_{ac} + c_j/c_a}{1 + c_j/c_a}$	3.17	72
M_c	$\dfrac{M_{ac}}{1 + c_j/c_a}$	2.46	66
$M_c{}''$	$\dfrac{M_{ac} - c_j/c_a}{1 + c_j/c_a}$	1.75	55
M_O	$\dfrac{M_c' + M_c}{2}$	2.81	69
M_κ	$\sqrt{M_{ac}}$	2.91	70

Figure 7 shows the measured overall directivity from each station at TRACERS (a) and NAOS (b). The directivity is calculated over 1 s blocks from a common distance of 100 D_{eff}. Increasing the block size and overlap between blocks provide additional data smoothing; however, a 1 s block size is used here to provide finer temporal or angular resolution. The abscissa is limited from 85° to 10° because the elevations of each station differed and vehicle pitches over rapidly. As a result, not all locations experienced the full 0° – 90° angular bandwidth.

There are several things to note about Figure 7a and b. First, the peak directivity angle, θ, varies with station location and launch, ranging from ~58° – 72°. This is partially due to the small block size. As a result, a decibel

average of the directivity curves from each launch was calculated and is plotted in both Figure 7 and Figure 8. From Figure 8, the peak directivity angle is shown to be 64° for both launches, which matches prior results, for Falcon 9 [21] and other rockets. For SLS, θ was found to be 66°, and Antares 230, a much smaller rocket, was found to have θ between 60° and 70°. However, it is noteworthy that the station-averaged peak directivity region in Figure 7 is extremely flat, with the 1 dB-down region spanning 58° – 72°.

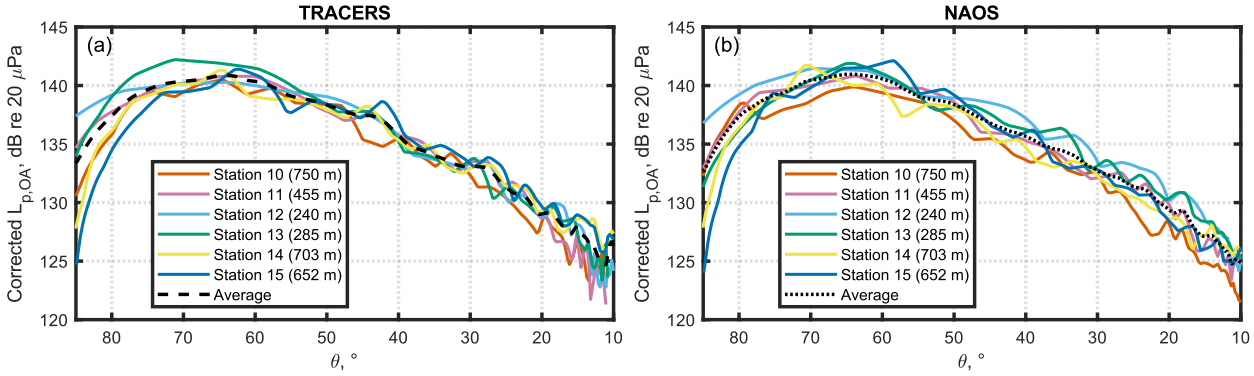

Figure 7. Falcon 9 overall sound pressure levels corrected to 100 D_{eff} as a function of polar angle (θ) using measured data (240 – 750 m) from the TRACERS (a) and NAOS (b) launches plotted against a decibel average of the curves.

Comparing the measured θ to the predicted θ_M in Table 3 provides insights into the width of this peak region. The predicted θ_M range from 55° – 72°, very similar to the 1 dB down region of the measured data. M_c', M_O, and M_κ predict $\theta_M \approx 70°$, an overestimate when compared to the measured Falcon 9 datasets. For M_κ, it follows that the present expression slightly overpredicts θ. Gee *et al.* [47] showed that for M_κ, while accurate within $\pm 5°$ for a broad range of jet conditions, all three rocket datapoints fell below the adopted expression of $M_\kappa \approx \sqrt{M_{\mathrm{ac}}}$. It is possible that supersonic instability waves radiate as Mach waves under rocket conditions, shifting the directivity lobe farther aft. M_c predicts 66.0° and most closely aligns with the measured θ of 64°. It is perhaps surprising that M_c'' predicts $\theta_M \approx$ 55°, which is 10° less than the average, measured θ_M, but not significantly different from some of the individual measurements in Figure 7 and is well within the average 3 dB down region relative to the maximum radiation angle (48° – 79°). Although some studies suggest that subsonic instability waves are not radiating phenomena [47], if they do radiate, they may contribute to the principal radiation lobe for Falcon 9.

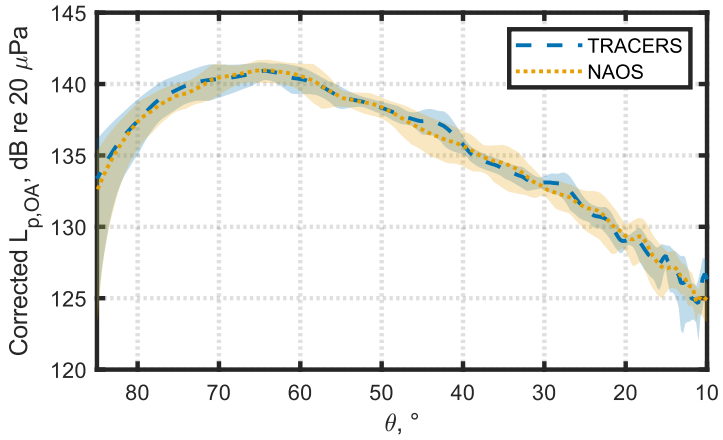

Figure 8. The decibel average directivity curves from Figure 7 for two Falcon 9 launches. Shaded regions represent $\pm$ 1 standard deviation.

Some data-processing assumptions could also be potential reasons for the mismatch between the measured and predicted directivity angles. These include an assumed source location (18 D_{eff}) downstream of the nozzle exit plane, the use of straight-ray propagation, and the neglect of moving-source effects. Ray tracing, for example, has shown

that the straight-ray propagation assumption can overestimate directivity angles by 2 – 3° [50]. Further investigation into these assumptions may provide additional insight into convective Mach number predictions of directivity angles.

While overall directivity is important in understanding the noise in the maximum radiation direction, frequency dependent directivity can provide additional information [53] [54]. It is useful to express frequency dependent directivity indices in terms of the directivity index, defined as the ratio of the acoustic intensity at a given frequency and angle to the intensity produced by an omnidirectional source with the same acoustic power. Typically represented in decibels, a positive directivity index indicates greater acoustic intensity along that angle and a negative directivity index represents less acoustic intensity. Falcon 9 frequency-dependent directivity indices are expressed in terms of Strouhal number, $Q(\theta, \mathrm{Sr})$, and shown in Figure 9a. The decibel average of all six measurement locations from both launches is plotted. Arrows in Figure 9a indicate select Sr plotted in Figure 9b. The results in Figure 9 were calculated using a longer block size (4 s) with 75% overlap to allow for enough averaging time down to 1 Hz. Using a block size between 1 and 4 s with 0 – 75% overlap yields result that are within 2° for peak directivity peak angle.

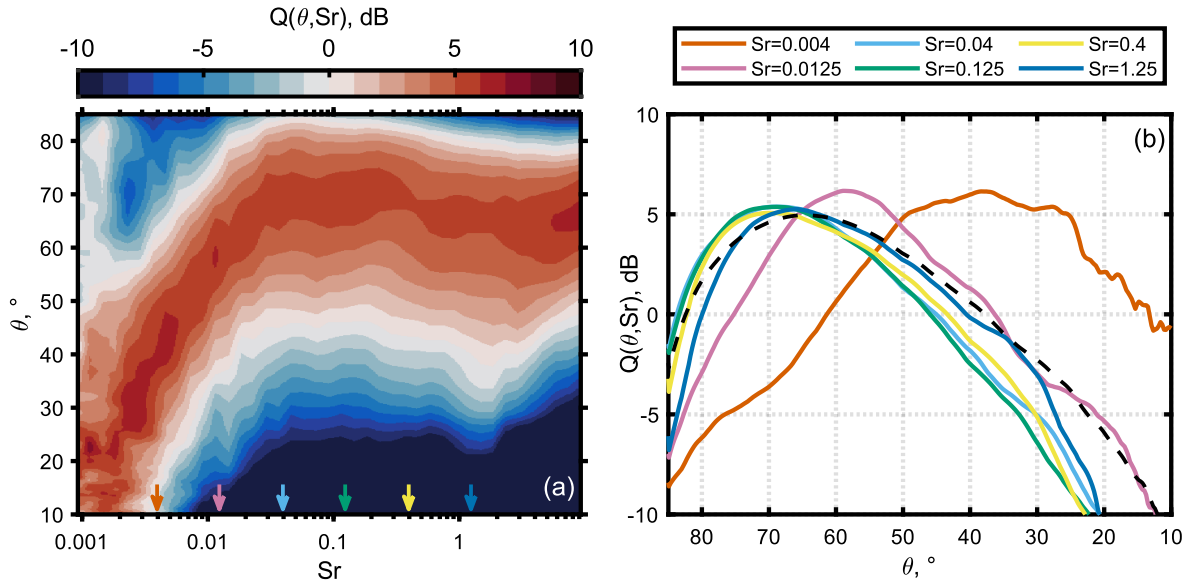

Figure 9. (a) Frequency dependent directivity indices for Falcon 9, decibel averaged over six stations and between two launches. Arrows indicate the select Strouhal numbers plotted in (b). The dashed line in (b) represents the overall directivity index.

In Figure 9a, the lowest frequencies ($< \mathrm{Sr} = 0.004$) peak at the shallowest angles, emerging between 10 – 30 °. As Sr increases, the radiation angle moves from the plume centerline towards the nozzle exit plane. At $\mathrm{Sr} = 0.004$, the noise is radiated at ~38° and, at $\mathrm{Sr} = 0.0125$, the noise is radiated at ~60°. The maximum $Q(\theta, \mathrm{Sr})$ is 6 dB at both frequencies. Beyond $\mathrm{Sr} = 0.0125$, all frequencies seem to peak between 60 and 75°. This is within range of most of the predicted θ_M in Table 3. Because most frequencies peak within this range, this provides additional evidence that both Kelvin-Helmholtz ($\theta_M = 72°$) and supersonic ($\theta_M = 66°$) instability waves are radiating from the jet. The final thing to note from Figure 9b is that the overall directivity index is plotted as a black, dashed line. The directivity index reaches a maximum at 64°, identical to the peak over the overall directivity in Figure 8, and the maximum $Q(\theta, \mathrm{Sr}) = Q_{\mathrm{max,OA}} = 5$ dB. This provides an important validation for the most recent implementation of the McInerny Model [38], given in Equation 1, where $Q_{\mathrm{max,OA}}$ was assumed to be 5 dB.

X. Sound Power

Another fundamental aeroacoustic analyses is the source's overall sound power level ($L_{w,\mathrm{OA}}$), which quantifies the total amount of sound energy radiated by the vehicle per unit time. $L_{w,\mathrm{OA}}$ can be estimated using the rocket's mechanical power (W_m), which is proportional to the vehicle's thrust and exit velocity. As per Equation 1, the estimated sound power is

$$L_{w,\mathrm{OA}} = 10\log_{10}\left(\frac{\frac{1}{2}\eta F U_e n}{W_{\mathrm{ref}}}\right), \tag{3}$$

where F is the thrust of one engine, U_e is the exit velocity, n is the number of engines, and W_{ref} = 1 pW. Using the same parameters as Section VI, η = 0.33% and the predicted $L_{w,\mathrm{OA}}$ is 195.7 dB.

The $L_{w,\mathrm{OA}}$ predictions can be confirmed by educing this quantity using measured data. Because the rocket is a moving acoustic source, trajectory data are used to track the location of the vehicle relative to the single, stationary microphone. This approach differs from traditional sound power calculations, which assume a stationary source measured using an array of microphones. However, it has proven to reliably quantify $L_{w,\mathrm{OA}}$ for an increasing number of rockets [21] [56] [57] [19]. Here, $L_{w,\mathrm{OA}}$ was calculated from the six near-pad measurements for the two launches using the methodology outlined by Anderson [56].

Table 4. Falcon 9 overall sound power levels using measured data (240 – 750 m) from two launches.

	TRACERS		NAOS	
Station	$\boldsymbol{L_{w,\mathrm{OA}}}$, dB re 1 pW	$\boldsymbol{\eta}$, %	$\boldsymbol{L_{w,\mathrm{OA}}}$, dB re 1 pW	$\boldsymbol{\eta}$, %
10 (750 m)	194.7	0.26	194.3	0.24
11 (455 m)	195.5	0.31	195.3	0.30
12 (240 m)	196.0	0.35	196.6	0.40
13 (285 m)	196.5	0.39	195.5	0.31
14 (703 m)	195.0	0.28	194.9	0.27
15 (652 m)	194.9	0.27	195.4	0.31
Average	**195.4**	**0.31**	**195.3**	**0.30**

Table 4 presents the calculated $L_{w,\mathrm{OA}}$ and corresponding η. Based on these data, Falcon 9's (decibel) average $L_{w,\mathrm{OA}}$ is 195.4 dB and η = 0.30%, with standard deviations of $\pm$0.7 dB and $\pm$0.05% respectively. Falcon 9's updated value of η differs from the historical assumption of 0.5% from NASA SP-8072 [6]. However, high-fidelity acoustic data from modern rockets [21] [56] [57] have increasingly conflicted with this value, which has been found to be much lower than the SP-8072 assumption.

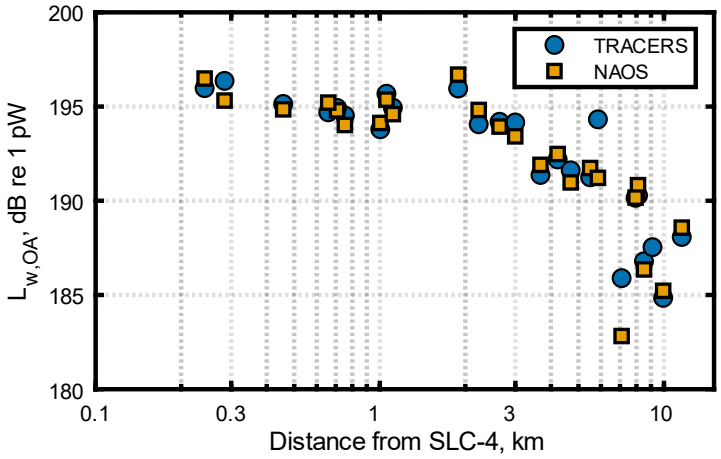

Figure 10. Overall sound power level as a function of distance from the launchpad for two Falcon 9 launches.

Although additional measurement locations were not used in the aeroacoustic analysis, sound power was calculated at every station and is shown out to 15 km in Figure 10. The $L_{w,\mathrm{OA}}$ is consistent (within 2 dB) out to approximately 2 km, where additional datapoints around ~1 km have $L_{w,\mathrm{OA}}$ greater than the average of 195.4 dB. Past

this measurement distance, there is a clear distance-dependence in sound power, which corresponds with what has been observed in the past for other rockets [22] [57]. Nonlinear propagation effects have been hypothesized as a possible cause of this decay [22] [56], but a rigorous analysis has yet to be performed to test this hypothesis. However, variation in the subset of data presented in this paper are likely due to a combination of terrain and local refraction effects as well as measurement uncertainty, not distance-dependent decay.

Prior Falcon 9 far-field measurements [21] suggested $L_{w,\mathrm{OA}}$ = 196 dB with η = 0.34%, nearly identical to the prediction from Equation 1. However, the acoustic data from this paper were collected ~6 – 12 km from SLC-4, and the sound power calculation did not explicitly account for ground reflections, which would decrease the predicted from 196 dB to 193 – 194 dB. As the calculated $L_{w,\mathrm{OA}}$ is known to decay over large distances, the measurements from TRACERS and NAOS collected 240 – 750 m from SLC-4 provides a more accurate source characterization with greater physicality over prior estimates.

The same methodology used to find $L_{w,\mathrm{OA}}$ can be applied to each individual frequency band to derive the sound power spectrum, L_w. In Figure 11, the L_w for the six stations measured during TRACERS (a) and NAOS (b) is plotted alongside a decibel-average of the curves. Within each launch, the spectra collapse at low frequencies (< 20 Hz) with less than 3 dB variation from the average.

The spectra in Figure 11a and b peak at various frequencies between 20 – 40 Hz, with the average curves peaking at 40 and 31.5 Hz for TRACERS and NAOS, respectively. For TRACERS, the peak region is rather flat, and extends from 20 – 40 Hz, which could explain the difference between these peaks. To compare with other vehicles, SLS's L_w has a lower peak frequency, around 17 Hz [57], whereas a T-7A military jet operating at afterburner has a peak frequency of ~100 Hz [59].

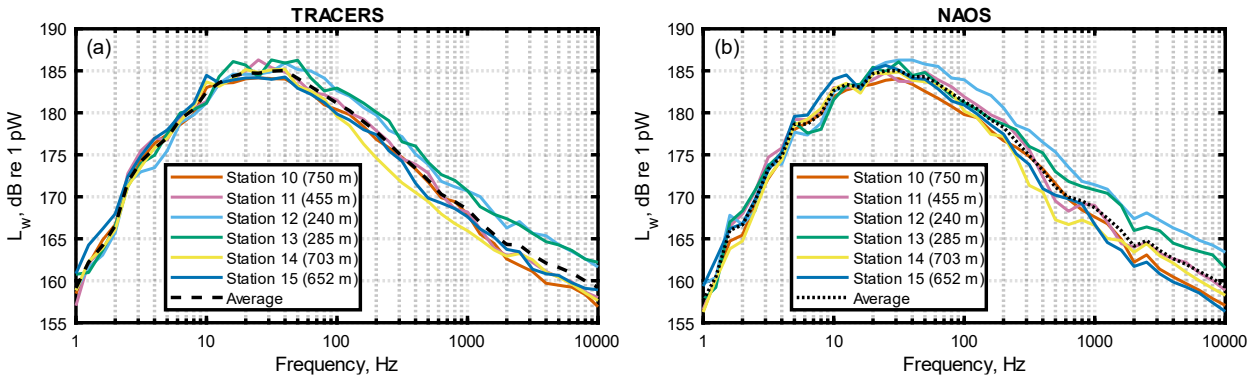

Figure 11. Falcon 9 one-third-octave sound power level spectra using measured data (240 – 750 m) from the TRACERS (a) and NAOS (b) launches plotted against a decibel average of the curves.

The Falcon 9 L_w begin to diverge past this the peak region, with stations closer to the pad (12 and 13) containing greater high-frequency energy than stations farther away from SLC-4. At 2 kHz, the L_w span a 6 dB range, representing a quadrupling in power. These high-frequency differences are responsible for the variation in $L_{w,\mathrm{OA}}$. While high-frequency loss is expected during long-range atmospheric propagation, it is surprising that such significant loss occurs even at stations less than 1 km from SLC-4. Variation in high frequency energy (~5 dB) was observed in SLS data measured at 1.5 km as well, but it was speculated that this trend was due to azimuthal asymmetry originating from the vehicle's multi-core configuration [57]. Falcon 9, with its nine plumes that merge almost instantly, should not generate azimuthally dependent noise, which makes the results observed at Stations 12 and 13 curious. Another possible reason for this variation at high frequencies is atmospheric turbulence, which has been shown to cause significant variation in aircraft sonic boom measurements beginning at ~30 Hz [58]. Together, SLS and Falcon 9's L_w provide motivation for future measurements to quantify the high-frequency distance dependence of L_w.

To study Falcon 9 in the context of other supersonic jets, the L_w is scaled by Strouhal number (Sr), defined as the ratio of the exit diameter (D_e) and the exit velocity (U_e). It is common to use exit parameters instead of fully expanded parameters for rockets because the exit values are typically easier to obtain. Mathews and Gee [38] showed that using exit instead of fully expanded parameters has a negligible effect. The average L_w from Figure 11a and b, normalized to $L_{w,\mathrm{OA}}$, converted to autospectral density units, and scaled by Sr, are plotted in Figure 12 alongside two predicted rocket spectra. The calculated averages from TRACERS and NAOS measurements agree well and are nearly indistinguishable from each other. Both Falcon 9 L_w are also nearly identical to the SATURN predictions, providing additional validation for the results in Section VII. The SATURN and measured L_w have a peak Sr of 0.011 and 0.010,

respectively. This is lower than SLS which had Sr = 0.015. The predicted curve from SP-8072 peaks at Sr = 0.02, different from the measured Falcon 9 data and SATURN predictions.

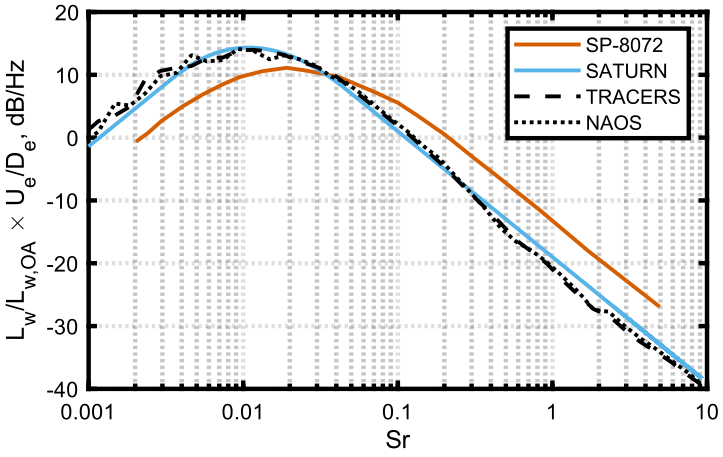

Figure 12. Normalized narrowband sound power spectra on a Strouhal number scale from SP-8072, SATURN, and two measured Falcon 9 launches (TRACERS & NAOS).

XI. Scaled Sound Pressure Levels

There are several methods for predicting $L_{\max}$ with the most well-known of these being the McInerny model mentioned in Section VI. However, measured data can also be extrapolated inward or outward to determine $L_{\max}$ at a desired distance. For data collected within ~5 km of the launchpad, geometric spreading can be used, as it accurately captures the far-field propagation at short distances. This is evident in Figure 5a, where the McInerny model fits the data well out to 5 km and then begins rolling off faster than spherical spreading would predict. We caution against using spherical spreading to extrapolate closer than the present measurement distances, as the near-field acoustic environment is complicated by non-spherical spreading, additional noise sources present during liftoff. Additionally, 5.8 dB ($\delta = 1.9$) was subtracted from these extrapolations to account for pressure doubling from ground-based measurements.

Table 5. Falcon 9 maximum overall sound pressure levels scaled to 100 D_{eff} (276 m) using measured data (240 – 750 m) from two launches.

	TRACERS	NAOS
Station	$L_{\max}$, dB re 20 μPa	$L_{\max}$, dB re 20 μPa
10 (750 m)	141.8	141.2
11 (455 m)	142.2	142.2
12 (240 m)	141.9	143.0
13 (285 m)	143.4	143.4
14 (703 m)	142.7	142.8
15 (652 m)	142.8	143.7
Average	**142.5**	**142.7**

To determine where Falcon 9 falls among other supersonic jets, $L_{\max}$ was scaled to 100 D_{eff}. These levels are given in Table 5, producing an average of 142.6 dB, with a standard deviation of $\pm$0.7 dB. A similar analysis was conducted previously for Falcon 9 by extrapolating data from 6 – 12 km to 100 D_{eff} [21]. Their paper showed an average $L_{\max} =$ 143 dB, which is remarkably similar to the results presented in this paper despite their long-range measurement distances. The likely cause of this agreement is that Mathews *et al.* [21] did not subtract 5.8 dB to account for a ground-based measurement. Accounting for these additional losses would adjust their value to $L_{\max} \approx$ 137 dB. This discrepancy is more intuitive, as significant losses, beyond just geometric spreading, are expected at large distances. For Starship Super Heavy, $L_{\max}$ has been found to vary by up to 3 – 4 dB between launches at 10 km [39]. Therefore, propagating measurements at 6 – 12 km inward to 100 D_{eff} should underpredict measured levels, as not all of the energy losses are being restored.

A final check of the values presented in Table 5 uses measured data from Station 13, located ~ 103 D_{eff} from SLC-4. The average $L_{\max}$ at this location from both launches, shown in Figure 5, is 147.2 dB. Subtracting 5.8 dB for ground reflections produces 141.4 dB, which is within 1.2 dB of the average distance-corrected $L_{\max}$.

Regarding scaled $L_{\max}$ for other rockets, SLS was found to have an $L_{\max} = 145.4$ dB [18]. However, accounting for ground reflections would adjust this value to $L_{\max} = 139.6$ dB. Comparison between SLS and Falcon 9 at this scaled distance shows that Falcon 9 is ~3 dB greater, which is surprising given SLS's greater thrust. Recent work [56] has shown that SLS has a relatively low η compared to other launch vehicles, which could explain this disagreement. Other results are derived from horizontal static firings of solid rocket motors. The GEM-63 has a $L_{Z,\max}$ of 143 – 144 dB [61], and the RSRM ranges from ~141 – 142 dB at 100 D_{eff} [7]. However, it is difficult to compare these data to ground-based measurements from a moving rocket because static-fired rocket motors often impinge on the ground or are fired into a hillside and the acoustic data were collected with tripod-mounted microphones.

Falcon 9's $L_{\max}$ at 100 D_{eff} is compared to other subsonic and supersonic jets in Figure 13, where $L_{\max}$ is plotted as a function of the Oertel convective Mach number. Greska *et al*. [49] compiled data from several references and fit the dataset from subsonic jets through rockets with low M_O. In Figure 13, this fit is extrapolated to higher Mach numbers to enable comparison with measured Falcon 9 data. Greska *et al*. [49] notes that the fit changes slope at $M_O = 1$ and $M_O = 1.35$, corresponding to changes in U_j.

For subsonic conditions ($M_O < 1$), the radiated power from the jet is proportional to U_j^8, whereas, at supersonic conditions ($M_O > 1$), it scales as U_j^3. At higher Mach numbers, Greska's fit suggests that sound power is proportional to ~$U_j^{1.5}$. Whereas Greska *et al.* [49] suggest maximum levels scale with M_o, inclusion of several rocket datapoints in Figure 13 alongside Falcon 9's average $L_{\max}$ at 100 D_{eff} indicates no increase in corrected $L_{\max}$, despite Falcon 9's M_O being significantly greater than the historical rocket datapoints. This suggests a breakdown in the appropriateness of using M_O to scale jet sound levels.

The reason for this breakdown may be found in considering η. While M_O continues to increase with jet condition, η has long been believed to reach an asymptote of ≤1% for supersonic jets after increasing as U_j^5 in the subsonic regime [51] [52]. Since η is not dependent on U_j for supersonic jets, the sound power and distance corrected sound pressure level do not necessarily increase with larger M_O.

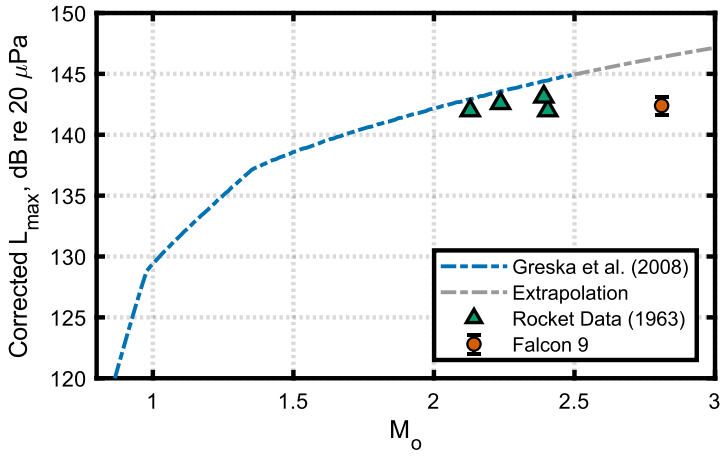

Figure 13. Maximum overall sound pressure levels, distance corrected to 100 D_{eff}, as a function of Oertel convective Mach Number. A fit of data from Greska *et al.* [49] has been reproduced and extrapolated to higher M_O. The rocket data included by Greska *et al.* are plotted as well as new data for Falcon 9.

XII. Conclusion

This paper has discussed an aeroacoustic analysis of SpaceX's Falcon 9 launch vehicle. A large-scale measurement campaign was conducted to characterize the acoustic events from two Falcon 9 launches with return-to-launch-site landings at Vandenberg Space Force Base. Key measurement results are summarized from the TRACERS and NAOS missions using data collected at 28 stations located 0.2 to 38.6 km from the launchpad (SLC-4). Four acoustic events are identified: ignition overpressure, maximum launch noise, flyback sonic boom, and maximum landing noise. Sound exposure level spectra corresponding to these events reveal that the launch noise spectrum has a peak frequency of 30

Hz, nearly an order of magnitude greater than the flyback sonic boom. Maximum 1-s averaged overall sound pressure levels from launch are nearly 150 dB at the closest measurement stations and collapse remarkably well between launches out to 38.6 km. SATURN predictions for running $L_{p,\mathrm{OA}}$ and one third octave band spectra are compared to measured data, validating this model for Falcon 9. Acoustic and trajectory data from both launches were combined to calculate the directivity and source sound power level at the six measurement locations less than 1 km from SLC-4. Falcon 9's average overall directivity has a wide, flat peak between 60 – 70°, which corresponds to convective Mach numbers for both Kelvin-Helmholtz and supersonic instability waves. On average, Falcon 9's sound power is 195.4 $\pm$ 0.7 dB (1σ) and its corresponding acoustic efficiency is 0.30%, similar to the efficiencies of most other modern rockets. Sound power spectra peak at a Strouhal number of 0.010, lower than the 0.02 assumed for rockets and significantly different than the 0.1 – 0.3 assumed for military jets. Maximum overall sound pressure levels at 100 D_{eff} are 142.6 $\pm$ 0.7 dB (1σ), which is similar to lower Mach number rockets. This provides evidence that acoustic efficiency does not increase with increasing convective Mach number for highly supersonic jets. The comprehensive dataset collected from two launches has advanced understanding Falcon 9's aeroacoustic properties, and future work should incorporate additional launches to validate and extend these results.

Appendix

Merlin 1D engine parameters were estimated using a combination of released data from SpaceX, and NASA's CEARUN program [23]. CEARUN has been used to provide reliable rocket engine parameters for other liquid-fueled engines, including the BE-4 and RD-180 [38]. CEARUN has also been used for the Merlin 1D in previous acoustic analyses [21]. However, some of these parameters are updated here to reflect recent engine development. Input parameters for the CEARUN model are given in Table 6. The inputs were gathered from a variety of online sources.

Table 6. CEARUN inputs for the Merlin 1D engine.

Ambient pressure (kPa)	101.3
Chamber pressure (MPa)	10.8
Supersonic area ratio	16
Oxidizer/fuel ratio	2.36
Fuel	RP-1
Oxidizer	02(L)
Run Condition	Frozen, NFZ=1

The Merlin's thrust is the only engine parameter released on SpaceX's official website, and this value is propagated in this paper. Throat diameter was used to derive the exit and fully expanded diameters, which match Mathews *et al*. [21]. All other parameters are direct outputs of the CEANRUN model.

SpaceX is constantly optimizing the Merlin 1D engine to increase Falcon 9's thrust and efficiency. While it is unclear what iteration of the Merlin 1D engine was flown on the TRACERS and NAOS missions, small changes in engine parameters likely have an insignificant impact on the generated noise and the aeroacoustic scalings discussed in this paper. For instance, a 10% increase in overall vehicle thrust corresponds to a 0.4 dB increase in $L_{w,\mathrm{OA}}$. The parameter estimates derived here represent the best estimate of the 2025 Merlin 1D engine and are likely sufficient for the results derived from this analysis.

Acknowledgments

The authors would like to acknowledge Dr. Logan T. Mathews for his advisement on running and testing the SATURN model.

This research is based upon work supported by the National Science Foundation Graduate Research Fellowship under Grant No. 2238458. Any opinions, findings, and conclusions or recommendations expressed in this material are those of the authors and do not necessarily reflect the views of the National Science Foundation. This work was also supported by Space Launch Delta 30 at Vandenberg Space Force Base, as part of a collaborative project with Dr. Lucas K. Hall at California State University Bakersfield.

References

[1] Cole, J. N., Von Gierke, H. E., Kyrazis, D. T., Eldred, K. M., and Humphrey, A. J., "Noise radiation from fourteen types of rockets in the 1,000 to 130,000 pounds thrust range," Wright Air Development Center Technical Report 57-354, AD 130794, 1957.

[2] Guest, S. H., and Jones, J. H., “Far-field acoustic environmental predictions for launch of Saturn V and Saturn V MLV Configuration,” NASA TN D-4117, Washington, DC, 1967.
[3] Wilhold, G. A., Guest, S. H., and Jones, J. H., "A technique for predicting far-field acoustic environments due to a moving rocket sound source," NASA TN D-1832, Washington, DC, 1963.
[4] Mayes, W. H., Lanford, W. E., and Hubbard, H. H., “Near-field and far-field noise surveys of solid-fuel rocket engines for a range of nozzle exit pressures,” NASA Report No. TN D-21, 1959. https://ntrs.nasa.gov/citations/19890068228
[5] Ffowcs Williams, J. E., “The noise from turbulence convected at high speed,” Philos. Trans. R. Soc., A 255(1061), 469–503, 1963. https://doi.org/10.1098/rsta.1963.0010
[6] Eldred, K. M., “Acoustic loads generated by the propulsion system,” NASA SP-8072, 1971.
[7] Lubert, C. P., Gee, K. L., and Tsutsumi, S., “Supersonic jet noise from launch vehicles: 50 years since NASA SP-8072,” *Journal of the Acoustical Society of America*, Vol. 151, No. 2, 2022, pp. 752–791. https://doi.org/10.1121/10.0009160
[8] Henderson, B., Gerhart, C., Jensen, E., Griffin, S., and Lazzaro, A., “Vibro-acoustic launch protection experiment (VALPE),” *Journal of the Acoustical Society of America*, Vol. 114, No. 4, 2003, p. 2384. https://doi.org/10.1121/1.4809177
[9] Griffin, S., Lane, S., and Leo, D., “Innovative vibroacoustic control approaches in space launch vehicles,” *Proceedings of INTER-NOISE 2000*, pp. 3583–3590. https://ince.publisher.ingentaconnect.com/content/ince/inceep/2000/00002000/00000004/art00033
[10] Jones, N., “Does the roar of rocket launches harm wildlife? These scientists seek answers,” *Nature*, Vol. 618, 2023, pp. 16–17. https://doi.org/10.1038/d41586-023-01713-7
[11] Gee, K. L., McLaughlin, B. W., Mathews, L.T., Edgington-Mitchell, D., Hart, G.W., and Anderson, M.C., “Launch Vehicle Noise and Australian Spaceports,” *Proceedings of Meetings on Acoustics*, Vol. 52, No. 1, 2023, Paper 040002. https://doi.org/10.1121/2.0001856
[12] Gee, K. L., Lubert, C.P., and James, M.M., “The roar of a rocket,” *Physics Today*, Vol. 77, No. 3, 2024, pp. 46–47. https://doi.org/10.1063/pt.izel.cyox
[13] McInerny, S. A., “Characteristics and predictions of far-field rocket noise,” *Noise Control Engineering Journal*, Vol. 38, No. 1, 1992, pp. 5–16. https://doi.org/10.3397/1.2827802
[14] McInerny, S. A., “Launch vehicle acoustics Part 1: Overall levels and spectral characteristics,” *Journal of Aircraft*, Vol. 33, No. 3, 1996, pp. 51–517. https://doi.org/10.2514/3.46974
[15] McInerny, S. A., “Launch vehicle acoustics Part 2: Statistics of the time domain data,” *Journal of Aircraft*, Vol. 33, No. 3, 1996, pp. 518–523. https://doi.org/10.2514/3.46975
[16] McInerny, S. A., Wickiser, J. K., and Mellen, R. H., “Rocket noise propagation,” *American Society of Mechanical Engineers Noise Control and Acoustics Division*, No. 24, 1997, pp. 37–50. https://doi.org/10.1115/IMECE1997-1027
[17] McInerny, S. A. and Ölçmen, S. M., “High-intensity rocket noise: Nonlinear propagation, atmospheric absorption, and characterization,” *Journal of the Acoustical Society of America*, Vol. 117, No. 2, 2005, pp. 578–591. https://doi.org/10.1121/1.1841711
[18] Kellison, M. S., Gee, K. L., Coyle, W. L., Anderson, M. C., Mathews, L. T., and Hart, G. W., “Aeroacoustical analyses from the Space Launch System Artemis-I mission,” *Proceedings of the 30th AIAA/CEAS Aeroacoustics Conference, Rome, Italy*, 2024, AIAA Paper 2024-3033. https://doi.org/10.2514/6.2024-3033
[19] Pulsipher, N. L., Gee, K. L., and Hart, G. W., “Noise radiation asymmetries in the Delta IV Heavy rocket,” Submitted to the *32nd AIAA/CEAS Aeroacoustics Conference, Brussels, Belgium*, 2026.
[20] Mathews, L. T., Anderson, M. C., Gardner, C. D., McLaughlin, B. W., Hinds, B. M., McCullah-Boozer, M. R., Hall, L. K. and Gee, K. L., “An overview of acoustical measurements made of the Atlas V JPSS-2 rocket launch,” *Proceedings of Meetings on Acoustics*, Vol. 51, No. 1, 2023, p. 040003. https://doi.org/10.1121/2.0001768
[21] Mathews, L. T., Gee, K. L., and Hart, G. W., “Characterization of Falcon 9 launch vehicle noise from far-field measurements,” *Journal of the Acoustical Society of America*, Vol. 150, No. 1, 2021, pp. 620–633. https://doi.org/10.1121/10.0005658
[22] Mathews, L. T., “Acoustic Characterization and Modeling of Heated Supersonic Tactical Jet Aircraft and Launched Rockets,” Ph.D. Dissertation, Department of Physics and Astronomy, Brigham Young University, 2025, see Chapter 6. https://scholarsarchive.byu.edu/etd/11034/.
An updated version of this chapter has been submitted as a manuscript. See Mathews, L. T., Gee, K. L., Wall, A. T., and Rasband, R. D., “A Modern Empirical Model for Predicting Rocket Launch Noise,” Submitted to the *Journal of the Acoustical Society of America*, 2026.

[23] McBride, B. J., and Gordon, S., "CEARUN," 2004, available at https://cearun.grc.nasa.gov/ (Last viewed April 26, 2026).
[24] Marston, T. M., "Diffraction correction and low-frequency response extension for condenser microphones," M.S. Thesis, Graduate Program in Acoustics, Penn. State Univ., 2008.
[25] Rasband, R. D., Gee, K. L., Gabrielson, T. B., and Loubeau, A., "Improving low-frequency response of sonic boom measurements through digital filtering," *JASA Express Letters*, Vol. 3, No. 1, 2023, Paper 014802. https://doi.org/10.1121/10.0016751
[26] Gee, K. L., Novakovich, D. J., Mathews, L. T., Anderson, M. C., and Rasband, R. D., "Development of a Weather-Robust Ground-Based System for Sonic Boom Measurements," NASA/CR-2020-5001870, 2020. https://ntrs.nasa.gov/citations/20205001870
[27] Gee, K. L., Hart, G. W., Cunningham, C. F., Anderson, M. C., Bassett, M. S., Mathews, L. T., Durrant, J. T., Moats, L. T., Coyle, W. L., Kellison, M. S., and Kuffskie, M. J., "Space Launch System acoustics: Far-field noise measurements of the Artemis-I launch," *JASA Express Letters*, Vol. 3, No. 2, 2023, Paper 023601. https://doi.org/10.1121/10.0016878
[28] Gee, K. L., Pulsipher, N. L., Kellison, M. S., Mathews, L. T., Anderson, M. C., and Hart, G. W., "Starship super heavy acoustics: Far-field noise measurements during launch and the first-ever booster catch," *JASA Express Lett*. 4(11), 113601, 2024. https://doi.org/10.1121/10.0034453
[29] Cami, R., Margasahayam, R., Nayfeh, J., and Thompson, K., "Rocket Launch-Induced Vibration and Ignition Overpressure Response," *International Congress on Sound and Vibration, Hong Kong*, 2001. https://ntrs.nasa.gov/citations/20020002698.
[30] Ryan, R. S., Jones, J. H., Guest, S. H., Struck, H. G., Rheinfurth, M. H., and Verferaime, V. S., "Propulsion system ignition overpressure for the Space Shuttle," NASA-TM-82458, 1981. https://ntrs.nasa.gov/citations/19820011425
[31] Gee, K. L., Russavage, P. B. Neilsen, T. B., Swift, S. H., and Vaughn, A. B., "Subjective rating of the jet noise crackle percept," *J. Acoust. Soc. Am.* 144(1), EL40–EL45, 2018. https://doi.org/10.1121/1.5046094
[32] Gee, K. L., "A review of jet crackle," *Proceedings of the 24th International Congress on Acoustics in Gyeongju, Korea*, 2022.
[33] Anderson, M. C. and Gee, K. L., "Why does the Falcon-9 booster make a triple sonic boom during flyback? An initial analysis," *JASA Express Lett.* 5(2), 023601, 2025. https://doi.org/10.1121/10.0035649
[34] Anderson, M. C. and Gee, K. L., "Modeling the SpaceX Falcon-9 Booster'sTriple Sonic Boom Using Multiple Models and Conditions," *Proceedings of AIAA Aviation Forum and ASCEND 2025, Las Vegas, NV*, 2025, AIAA Paper 2025-3081. https://doi.org/10.2514/6.2025-3081
[35] Anderson, M. C., and Gee, K. L., "Sonic boom measurements from the SpaceX Transporter-8 Falcon-9 rocket landing at Vandenberg Space Force Base," *Proceedings of the 30th AIAA/CEAS Aeroacoustics Conference, Rome, Italy*, 2024, AIAA Paper 2024-3188. https://doi.org/10.2514/6.2024-3188
[36] Durrant, J. T., Anderson, M. C., Bassett, M. S., Gee, K. L., Hart, G. W., Batelaan, R. H., Lawrence, D. C., and Hall, L. K., "Overview and spectral analysis of the Falcon-9 SARah-1 launch and reentry sonic boom," *Proceedings of Meetings on Acoustics*, Vol. 51, No. 1, 2023, p. 040006. https://doi.org/10.1121/2.0001767
[37] Blackstock, D. T., Hamilton, M. F., and Pierce, A. D., "Progressive waves in lossless and lossy fluids," in Nonlinear Acoustics, 2024, edited by M. F. Hamilton and D. T. Blackstock (Springer, Cham, Switzerland), pp. 63–147.
[38] Mathews, L. T. and Gee, K. L., "Methods for predicting overall sound power and maximum overall sound pressure levels from heated supersonic jets, including rockets," *J. Acoust. Soc. Am.*, 158(1), 371–379, 2025. https://doi.org/10.1121/10.0037192
[39] Gee, K. L., Pulsipher, N. L., Kellison, M. S., Hart, G. W., Mathews, L. T., and Anderson, M. C., "Starship Super Heavy acoustics: Comparing launch noise from Flights 5 and 6," *JASA Express Lett*. 5(2), 023602, 2025. https://doi.org/10.1121/10.0035925
[40] Loubeau, A., and Page, J., "Human Perception of Sonic Booms from Supersonic Aircraft Advances in Human Response," *Acoustics Today*, Vol 15, Issue 3, 2018.
[41] Anderson, M. C., Gee, K. L., and Nyborg, K., "Flyback sonic booms from Falcon-9 rockets: Measured data and some considerations for future models," *Proceedings of Meetings on Acoustics*, Vol. 54, No. 1, 2024, Paper 040005. https://doi.org/10.1121/2.0001916
[42] Bradley, K. A., James, M. M., Salton, A. R., and Boeker, E. R., "Commercial Space Operations Noise and Sonic Boom Modeling and Analysis," National Academies of Sciences, Engineering, and Medicine Transportation Research Board, Washington, DC, 2018. https://onlinepubs.trb.org/onlinepubs/acrp/acrp_wod_051RumbleGuide.pdf

[43] Jordan, P. and Colonius, T., "Wave Packets and Turbulent Jet Noise," *Annual Review Fluid Mechanics*, Vol. 45, 2013, 173-195. https://doi.org/10.1146/annurev-fluid-011212-140756
[44] Oertel, H., "Machwave Radiation of Hot Supersonic Jets Investigated by Means of the Shock Tube and New Optical Techniques," *12th International Symposium on Shock Tubes and Waves*, July 1980, pp. 266–275.
[45] Oertel, H., "Measured Velocity Fluctuations Inside the Mixing Layer of a Supersonic Jet," *Recent Contributions to Fluid Mechanics*, Vol. 1, 1982, pp. 170–179.
[46] Tam, C. K. W., and Hu, F. Q., "On the Three Families of Instability Waves of High-Speed Jets," *Journal of Fluid Mechanics*, Vol. 201, April 1989, pp. 447–483. https://doi.org/10.1017/S002211208900100X
[47] Gee, K. L., Olaveson, T. W., and Mathews, L. T., "Convective Mach Number and Full-Scale Supersonic Jet Noise Directivity," *AIAA Journal*, Vol. 63, No. 4, 2025, pp. 1393–1404. https://doi.org/10.2514/1.J064208
[48] Greska, B. J., "Supersonic Jet Noise and Its Reduction Using Microjet Injection," Ph.D. Dissertation, Florida State Univ., Tallahassee, FL, 2005.
[49] Greska, B., Krothapalli, A., Horne, W. C., and Burnside, N., "A Near-Field Study of High Temperature Supersonic Jets," *Proceedings of the 14th AIAA/CEASAeroacoustics Conference Vancouver, British Colombia*, 2008, AIAA Paper 2008-3026. https://doi.org/10.2514/6.2008-3026
[50] Carlston, N. F., Gee, K. L., and Hart G. W., "Using ray tracing to predict far-field spectral time histories of Falcon 9 launch noise," *189th Meeting of the Acoustical Society of America, Honolulu, HI*, 2025. https://acousticalsociety.org/wp-content/uploads/2025/11/honolulu-programrevised1.pdf
[51] Franken, P. A., "Review of information on jet noise," *Noise Control*, Vol. 4, 1958, pp. 8–16. https://doi.org/10.1121/1.2369320
[52] Wall, A. T., Gee, K. L., Morris, P. J., Colonius, T., and Lowe, K. T., "Introduction to the Special Issue on Supersonic Jet Noise," *Journal of the Acoustical Society of America*, Vol. 151, No. 2, 2022, pp. 806–816. https://doi.org/10.1121/10.0009321
[53] James, M. M., Salton, A. R., Gee, K. L., Neilsen, T. B., McInerny, S. A., and Kenny, R. J, "Modification of directivity curves for a rocket noise model," *Proceedings of Meetings on Acoustics*, Vol. 18, No. 1, 2014, Paper 040008. https://doi.org/10.1121/1.4870986
[54] Hart, G. W., Gee K. L., and Cook, M. R., "Corrected frequency-dependent directivity indices for large solid rocket motors," *Proceedings of Meetings on Acoustics*, Vol. 51, No. 1, 2023, Paper 040007. https://doi.org/10.1121/2.0001810
[55] Gee, K. L., Whiting, E. B., Neilsen, T. B., James, M. M., and Salton, A. R., "Development of a near-field intensity measurement capability for static rocket firings," *Trans. JSASS Aerosp. Tech. Jpn.*, 2016, 14, Po_2_9–Po_2_15.
[56] Anderson, M. C., "Sonic Booms from Rockets: Measurements and Modeling," Ph.D. Dissertation, Department of Physics and Astronomy, Brigham Young University, 2026. https://scholarsarchive.byu.edu/etd/11192/
[57] Kellison, M. S. and Gee K. L., "Sound Power of NASA's lunar rockets: Space Launch System versus Saturn V," *JASA Express Letters*, Vol. 3, No. 11, 2023, Paper 113601. https://doi.org/10.1121/10.0022538
[58] Nyborg, K., Gee, K. L., and Loubeau, A., "Variation in Sonic Boom Metrics due to Atmospheric Turbulence during CarpetDIEM III," *Proceedings of AIAA Aviation Forum and ASCEND 2025, Las Vegas, NV*, 2025, AIAA Paper 2025-3080. https://doi.org/10.2514/6.2025-3080
[59] Pratt, H. J., Mathews, L. T., Olaveson, T. W., and Gee, K. L., "Sound power level spectra of an installed General Electric F404 engine," *JASA Express Lett.*, 5(4), 043601, 2025. https://doi.org/10.1121/10.0036464
[60] Kellison, M. S., Gee, K. L., Cunningham, C. F., Coyle, W. L., Moore, T. M., and Hart, G. W., "Community-based noise measurements of the Artemis-I mission," *Proceedings of Meetings on Acoustics*, Vol. 51, No. 1, 2023, Paper 040004. https://doi.org/10.1121/2.0001786
[61] Bassett, M. S., Gee, K. L., Hart, G. W., Mathews, L. T., Rasband, R. D., and Novakovich, D. J., "Peak directivity analysis of far-field acoustical measurements during three GEM 63 static firings," *Proceedings of Meetings on Acoustics*, Vol. 39, No. 1, 2021, Paper 040004. https://doi.org/10.1121/2.0001467